Journal of
Synchrotron Radiation

ISSN 0909-0495

Received 3 February 2009
Accepted 1 April 2009

Relationship between the structural distortion and the Mn electronic state in $La_{1-x}Ca_xMnO_3$: a Mn *K*-edge XANES study

Jesús Chaboy

Instituto de Ciencia de Materiales de Aragón and Departamento de Física de la Materia Condensada, CSIC-Universidad de Zaragoza, 50009 Zaragoza, Spain. E-mail: jchaboy@unizar.es

A theoretical study of the X-ray absorption near-edge structure (XANES) spectra at the Mn *K*-edge in the $La_{1-x}Ca_xMnO_3$ series is reported. The relationship between the edge shift, the Ca–La substitution and the distortion of the MnO_6 octahedra in these systems has been studied. It is shown that, by correctly considering these effects simultaneously, the experimental XANES data are consistent with the presence of two different Mn local environments in the intermediate $La_{1-x}Ca_xMnO_3$ compounds. By taking into account the energy shift associated with the modification of the MnO_6 distortion as Ca substitutes for La, it is possible to reproduce the XANES spectra of the intermediate-doped compounds starting from the experimental spectra of the end-members $LaMnO_3$ and $CaMnO_3$. These results point out the need to re-examine the conclusions derived in the past from the simple analysis of the Mn *K*-edge XANES edge-shift in these materials. In particular, it is shown that the modification of the Mn *K*-edge absorption through the $La_{1-x}Ca_xMnO_3$ series is well reproduced by considering the simultaneous presence of both distorted and undistorted octahedra and, consequently, that the existence of charge-ordering phenomena cannot be ruled out from the XANES data.

Keywords: X-ray absorption spectroscopy; XANES; *ab initio* calculation; manganese perovskites.

1. Introduction

Manganese oxides with perovskite structure have been the subject of a large number of theoretical and experimental studies in the last two decades owing to their peculiar magnetic, electronic and transport properties. $R_{1-x}A_xMnO_3$ compounds, in which R is a rare-earth element and A is a divalent ion like Ca, Sr or Ba, display, depending on composition, a diverse range of interrelated phenomena. These include ferromagnetic, antiferromagnetic, orbital and/or charge ordering, various phase transitions, colossal magnetoresistance *etc.* (Edwards, 2002; Dagotto *et al.*, 2001; Renner *et al.*, 2002). The competing interactions taking place in these materials result in a complex phase diagram in terms of structural, magnetic and electronic properties as a function of composition, temperature and pressure (Zener, 1951; Anderson & Hasegawa, 1955; de Gennes, 1960; Millis *et al.*, 1995, 1996; Salamon & Jaime, 2001).

The $La_{1-x}Ca_xMnO_3$ series exemplifies this complex behaviour (Schiffer *et al.*, 1995). These compounds are paramagnetic insulators at room temperature and doping with Ca leads to novel transport and magnetic properties including colossal magnetoresistance (CMR) and ferromagnetism (FM). For samples with Ca concentrations in the range $0.2 \leq x \leq 0.5$ the FM transition coincides with a metal–insulator transition (Schiffer *et al.*, 1995). At higher calcium concentrations, the system becomes antiferromagnetic being an insulator both above and below T_N. Moreover, this concentration region also exhibits charge ordering (Ramirez *et al.*, 1996; Chen *et al.*, 1997). The basic mechanism of electronic transport has long been thought to be the double-exchange mechanism (Zener, 1951; Anderson & Hasegawa, 1955; de Gennes, 1960). However, several features of the CMR materials, such as the resistivity data, are inconsistent with a model that only consists of double exchange. Therefore, other mechanisms, such as the spin-lattice interactions through a strong coupling of the carriers to Jahn–Teller (JT) lattice distortions, must be considered (Millis *et al.*, 1995, 1996). Indeed, neutron scattering experiments pointed out that the local atomic structure around Mn ions plays a crucial role in determining these complex phenomena (Radaelli *et al.*, 1997; Louca & Egami, 1999). Consequently, much attention has been given to short-range-order techniques like X-ray absorption spectroscopy (XAS) because they are capable of directly probing the local atomic structure. In this way, numerous EXAFS studies have faced the characterization of the MnO_6 octahedra and the

local lattice distortions through the $La_{1-x}Ca_xMnO_3$ series (Booth *et al.*, 1996, 1998; Lanzara *et al.*, 1998; Meneghini *et al.*, 1997, 2002; Subías *et al.*, 1998; Jiang *et al.*, 2007). Despite all these works using the same experimental technique, different schemes are proposed for both the local distortions and their interpretation in connection with their magnetic properties. As a consequence, there is no agreement of the microscopic description of the local structure in these doped manganites (for a survey see, for example, Subías *et al.*, 2002) and several problems, such as the temperature dependence of the distortion of the MnO_6 octahedra and the coexistence of distorted and undistorted MnO_6 octahedra, still remain open (Booth *et al.*, 1998; Subías *et al.*, 2002). According to Booth *et al.*, the oxygen environment around the manganese becomes less distorted as the calcium concentration is increased. The Mn–O distortions are consistent with a linear interpolation of the end-member compounds $LaMnO_3$ (Mn^{3+}) and $CaMnO_3$ (Mn^{4+}) in such a way that a model which includes a JT distortion in proportion to the Ca concentration fits the data well (Booth *et al.*, 1998). EXAFS analysis of these Mn–O distortions is consistent with a model where individual Mn^{3+} sites have strong JT distortions while Mn^{4+} sites do not (Booth *et al.*, 1998). In contrast, the interpretation of Subías *et al.* of similar data does not support the presence of an inhomogeneous mixture of Mn^{3+} and Mn^{4+} through the series (Subías *et al.*, 2002).

This controversy also extends to the analysis of the XANES part of the absorption spectra. XANES studies have shown that (i) the Mn *K*-edge spectra of the $La_{1-x}Ca_xMnO_3$ compounds have a similar shape for the whole series, and (ii) the edge shifts almost rigidly to higher energy as the Ca concentration is increased (Booth *et al.*, 1998; Subías *et al.*, 1997; Croft *et al.*, 1997; Bridges *et al.*, 2001). It is commonly argued that the sharpness of the edge is suggestive of a transition into a Mn state that is uniform throughout the sample (Booth *et al.*, 1998; Subías *et al.*, 1997). In this way, starting from a naive ionic model in which the electronic state is Mn^{3+} in $LaMnO_3$ and Mn^{4+} in $CaMnO_3$, the substitution of a divalent ion for La formally changes the average Mn valence to $3 + x$. This conjecture should also be supported by the fact that the observed Mn *K*-edge absorption of the intermediate $La_{1-x}Ca_xMnO_3$ compounds cannot be modelled as a weighted sum of the $LaMnO_3$ and $CaMnO_3$ spectra (Subías *et al.*, 1997; García *et al.*, 2001*b*). However, Ignatov *et al.* have pointed out that a model assuming only one type of manganese fails to reproduce the shake-up feature in the XANES or it assumes a structureless X-ray photoelectron spectrum, both inconsistent with experimental observations (Ignatov *et al.*, 2001). Moreover, Bridges *et al.* have suggested that using the position of the peak in the first derivative curve as a measure of the average edge position is only an approximate measure of the average edge shift (Bridges *et al.*, 2001). They have proposed an alternative method of obtaining a better estimate of the average edge shift with concentration, concluding that there is a splitting of the Mn—O distances. Therefore, although there is no modification of the sharpness of the edge, which is expected for two well defined valence states, there is evidence of a coexistence of undistorted and distorted MnO_6 octahedra, which indicates some change in the local charge distribution (Bridges *et al.*, 2001). A similar contest also extends to the interpretation of recent X-ray resonant scattering experiments in the so-called charge-ordered compounds (Subías *et al.*, 2002; Murakami *et al.*, 1998; Zimmermann *et al.*, 1999; Nakamura *et al.*, 1999). While the presence of two differently distorted MnO_6 octahedra in the charge-ordered manganites starts to be accepted (Jiang *et al.*, 2007; García *et al.*, 2001*a*), several authors conclude that these two kinds of Mn atoms cannot be regarded as pure ionic Mn^{3+} and Mn^{4+} ions and that no real Mn^{3+}/Mn^{4+} charge ordering occurs in these compounds (García *et al.*, 2001*a*).

Therefore, the occurrence of either charge localization, inhomogeneous Mn^{3+} and Mn^{4+} or homogeneous Mn^{3+x}, is still a matter of controversy. We have a scenario in which similar EXAFS and XANES results lead to opposite conclusions regarding the distortion of the local environment of the Mn ions through the $La_{1-x}Ca_xMnO_3$ series: (i) there is a mixture of ionic-like Mn^{3+} and Mn^{4+} ions in the materials or, on the contrary, (ii) all the Mn atoms in the substituted compounds show the same intermediate valence. Within the extended framework identifying the Mn electronic state with the distortion of the MnO_6 octahedron (Booth *et al.*, 1996, 1998; Lanzara *et al.*, 1998; Meneghini *et al.*, 1997, 2002; Subías *et al.*, 1997, 1998, 2002; Jiang *et al.*, 2007; Croft *et al.*, 1997; Bridges *et al.*, 2001; García *et al.*, 2001*b*), the first possibility implies the coexistence of distorted and undistorted MnO_6 octahedra such as those found in the parent $LaMnO_3$ and $CaMnO_3$ compounds (Booth *et al.*, 1998). By contrast, all the MnO_6 octahedra would be equally distorted in the second case, with all the Mn atoms showing an intermediate valence ranging between Mn^{3+} and Mn^{4+} (Subías *et al.*, 2002). If this is the case, both the valence and the distortion should evolve linearly through the $La_{1-x}Ca_xMnO_3$ series as a function of the doping.

This work is aimed at determining whether X-ray absorption spectroscopy at the Mn *K*-edge is capable of discerning between both aforesaid possibilities. In this way we have performed an extensive and systematic *ab initio* computation of the Mn *K*-edge in $LaMnO_3$, $CaMnO_3$ and the intermediate $La_{1-x}Ca_xMnO_3$ compounds within the multiple-scattering framework (Natoli & Benfatto, 1986). In particular, we have studied how the local distortion of the MnO_6 octahedra and the electronic state of Mn ions affect the Mn *K*-edge XANES spectra of the $La_{1-x}Ca_xMnO_3$ materials; in particular, how they are related to both the position of the absorption edge and the spectral shape. A comparison between the experimental data and *ab initio* computations based on multiple-scattering theory indicates that the election of the cluster size is critical in correctly reproducing all of the experimental XANES features. This need is independent of both the electronic state of the Mn atoms and the occurrence of distorted or undistorted MnO_6 octahedra. By fixing the same computational parameters, we have studied the relationship between the edge shift, the Ca–La substitution and the distortion of the MnO_6 octahedra through the series. Our analysis shows that

by taking into account these effects simultaneously it is possible to reproduce the spectra of the intermediate $La_{1-x}Ca_xMnO_3$ compounds. In this way we show that, by considering the variation of the edge shift associated with the modification of the MnO_6 distortion as La is substituted by Ca, it is possible to reproduce the XANES spectra of the intermediate-doped compounds starting from the experimental spectra of the end-member $LaMnO_3$ and $CaMnO_3$ compounds. These results show that the experimental XANES data are consistent with the presence of two different Mn local environments in the intermediate compounds, and point out the need to re-examine the conclusions derived in the past from the simple analysis of the Mn *K*-edge XANES edge-shift in these materials.

2. Computational methods

Computation of the Mn *K*-edge XANES spectra was carried out using the multiple-scattering code *CONTINUUM* (Benfatto *et al.*, 1986) based on the one-electron full-multiple-scattering theory (Lee & Pendry, 1975; Natoli & Benfatto, 1986). For a complete discussion of the procedure, we refer the reader to Chaboy & Quarteri (1995) and Natoli *et al.* (2003).

The potential for the different atomic clusters was approximated by a set of spherically averaged muffin-tin potentials built by following the standard Mattheis' prescription (Mattheis, 1964). The muffin-tin radii were determined following Norman's criterion (Norman, 1974). The Coulomb part of each atomic potential was generated using charge densities for neutral atoms obtained from the tabulated atomic wavefunctions of Clementi & Roetti (1974). We have also checked that using charge densities obtained from non-local self-consistent Dirac–Fock code (Ankudinov *et al.*, 1998; Desclaux, 1975) does not modify the results. The atomic orbitals were chosen to be neutral for the ground state potential, whereas different choices were used to build the final state potential. We have found during the present calculations that the screened and relaxed $Z+1$ option (Lee & Beni, 1977) leads to the best performance in simulating the experimental spectra. Finally, we have studied how the different choices for the exchange and correlation part of the final state potential affect the agreement between the experimental and *ab initio* calculated spectra. The calculated theoretical spectra have been further convoluted with a Lorentzian shape function to account for the core-hole lifetime (Γ = 1.2 eV) (Krause & Oliver, 1979) and the experimental resolution (Γ = 1 eV). The computed spectra have been compared with the experimental XANES data reported by Subías *et al.* (1997).

3. Results and discussion

The local structure of Mn in $CaMnO_3$ consists of six O atoms in a near regular octahedral geometry (see Fig. 1) in which four O atoms lie at R_1(Mn—O) = 1.89 Å from Mn, and the other two O atoms are located at a distance R_2(Mn—O) = 1.92 Å (Fawcett *et al.*, 1998). In the case of $LaMnO_3$, this

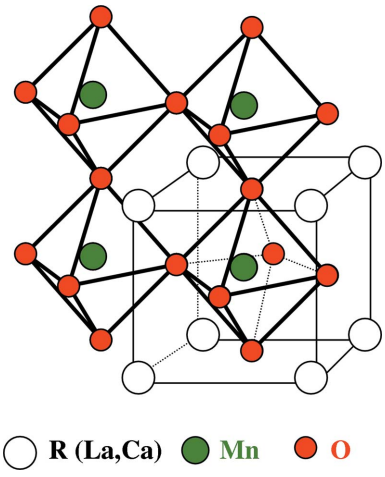

Figure 1
Schematic view of the $RMnO_3$ structure. This figure is in colour in the electronic version of this paper.

octahedron is distorted showing three different Mn—O pairs: R_1(Mn—O) = 1.91 Å, R_2(Mn—O) = 1.97 Å and R_3(Mn—O) = 2.18 Å (Iliev *et al.*, 1998). The distortion in $LaMnO_3$ is due to the JT effect associated with the $3d^4$ electronic configuration in O_h site symmetry of the Mn^{3+} ion. Such a JT distortion is absent in $CaMnO_3$ where only Mn^{4+} ions are present.

Previous fingerprint analysis of the Mn *K*-edge XANES spectra of the intermediate $La_{1-x}Ca_xMnO_3$ compounds ruled out the existence of a simple mixture of Mn^{3+} and Mn^{4+} ions in the substituted La–Ca manganite samples because the absorption edge shifts almost rigidly to higher energy as the concentration is increased. These works assumed that there is no distortion of the MnO_6 octahedra as the cell parameter varies. In this way, the spectra of the substituted compounds are compared with the weighted sum of the XANES spectra of the end compounds $LaMnO_3$ (Mn^{3+}) and $CaMnO_3$ (Mn^{4+}) (Booth *et al.*, 1998; Subías *et al.*, 1997; Croft *et al.*, 1997; Bridges *et al.*, 2001). However, one should expect that the modification of the interatomic distances associated with the La–Ca substitution affects the distortion of the MnO_6 octahedra. Consequently, the edge position should change because it is intimately linked to the local structure: when the bond length of a molecule lengthens, the position of the edge shifts to lower energy. Indeed, several authors have shown that, in the case of the $La_{1-x}Ca_xMnO_3$ systems, the Mn—O distortions are the primary producers of the polarization-dependent splitting of the main line (Benfatto *et al.*, 1999), so that the main line profile is a direct mirror of the degree of JT distortion (Qian *et al.*, 2001). In this respect, Benfatto *et al.* (1999) and Elfimov *et al.* (1999) have calculated, using different methods, that the edge should shift about 2 eV between the long and short bonds. Therefore, the modification of the cell parameters through the $La_{1-x}Ca_xMnO_3$ series may result in changes of the interatomic distances of the MnO_6 octahedra without modification of the electronic state of the Mn ions (Ramos *et al.*, 2007). If this is the case, the XAS spectra of the Mn^{3+} and Mn^{4+} ions in the modified crystal cell

structures of the intermediate compounds should differ from those of $LaMnO_3$ and $CaMnO_3$, respectively, and the above conclusions should be revised.

In an attempt to clarify this problem, we have studied how the local distortion of the MnO_6 octahedra affects the Mn *K*-edge XANES spectra of the $La_{1-x}Ca_xMnO_3$ materials. To this end we have performed a detailed *ab initio* computation of the Mn *K*-edge XANES through the $La_{1-x}Ca_xMnO_3$ series. The first objective has been to determine the necessary conditions to obtain an accurate reproduction of the experimental spectra of the end-members of the series, *i.e.* $LaMnO_3$ and $CaMnO_3$, in order to fix the same computational parameters for the computation of the $La_{1-x}Ca_xMnO_3$ systems. A complete discussion of the different aspects of these computations is detailed in Appendix *A*. The best agreement between the theoretical and experimental spectra for both $LaMnO_3$ and $CaMnO_3$ are reported in Fig. 2. Here, we briefly summarize the main conclusions of this starting study.

(i) The computations performed by increasing the cluster size indicate the need to include scattering contributions from the neighbouring atoms within at least the first 7 Å around the absorbing Mn atom in order to reproduce the experimental Mn *K*-edge spectra of both $LaMnO_3$ and $CaMnO_3$. Computations made for a cluster of 125 atoms yield an accurate reproduction of the high-energy spectral features in the first 60 eV above the edge. The computations performed for medium-size clusters ($r_{max} \leq 6$ Å) fail to reproduce the experimental spectra of both $LaMnO_3$ and $CaMnO_3$. This result demonstrates that special caution has to be given to strong conclusions, such as the non-existence of Mn^{3+}/Mn^{4+} charge ordering, based on computations performed on small clusters (García *et al.*, 2001*a*).

(ii) It is mandatory to use a high value of l_{max} in order to account for the spectral features (C, D and E) located between 30 and 60 eV above the edge.

(iii) These computations show the importance of the choice of the overlapping factor among the muffin-tin spheres. It does affect both the intensity and the spectral shape in the first 40 eV of the computed spectra, which results crucially in correctly reproducing the broad resonance B (B_1 and B_2 in the case of $CaMnO_3$). In this respect, computations performed by using a 1% factor show a better agreement with the experimental spectra than those corresponding to a 10% overlapping factor.

(iv) The best agreement with the experimental spectra is obtained by using complex potentials in which the imaginary part accounts for the photoelectron damping. In addition to the Hedin–Lundqvist (HL) potential we have also used the energy-dependent Dirac–Hara (DH) exchange potential (Natoli *et al.*, 2003) after adding the imaginary part of the HL (hereafter, complex Dirac–Hara). As shown in Fig. 2, computations made by using both potentials show a good agreement with the experimental data. In both the $LaMnO_3$ and $CaMnO_3$ cases, the HL potential yields the best reproduction of the intensity ratio of the main spectral features at low energy (A, B), while the complex DH improves the reproduction of the high-energy region (C, D and E features).

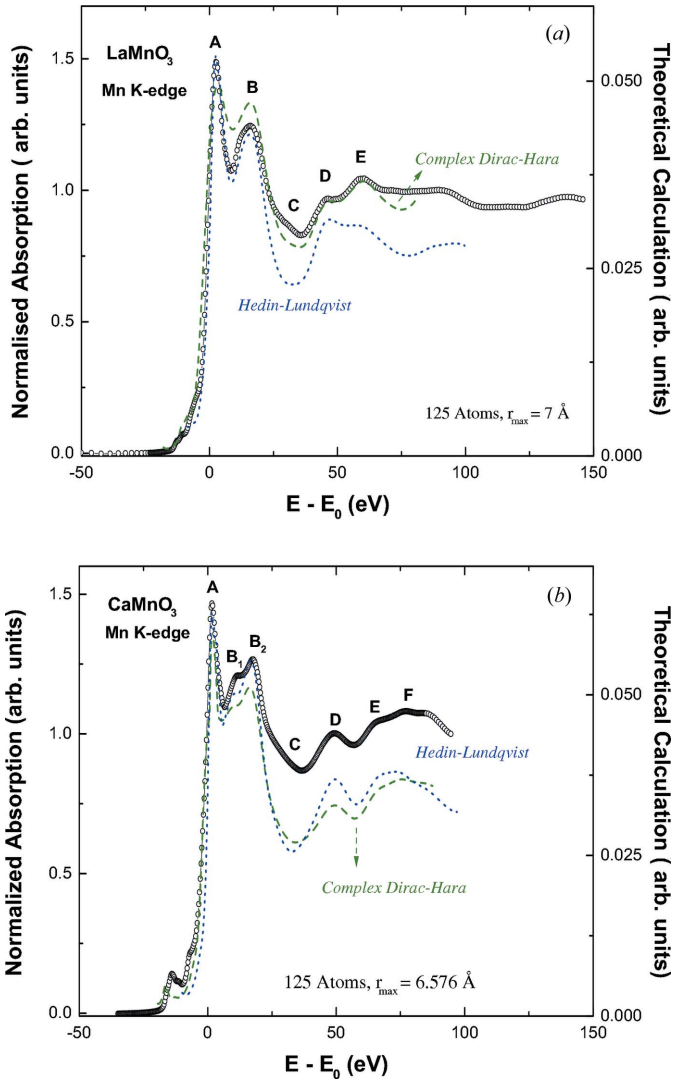

Figure 2
Comparison of the experimental Mn *K*-edge XANES spectra (open circles) of $LaMnO_3$ and $CaMnO_3$ and the theoretical spectra (green, dashed line) calculated on clusters containing 125 atoms by imposing an overlapping factor of 1% and l_{max} = 4 and by using complex ECP potentials (see Appendix *A* for details): HL (blue, dotted line) and complex DH (green, dashed line). This figure is in colour in the electronic version of this paper.

It should be noted that during the computations we have used the same charge densities for neutral Mn in both $LaMnO_3$ and $CaMnO_3$. The good agreement reached by the computations in the comparison with the experimental data indicate that the influence of the electronic state of Mn, Mn^{3+} or Mn^{4+} mainly affects the edge position. Indeed, it has been previously reported that the use of self-consistent-field (SCF) charge densities does not affect the spectral shape and that only the edge position is affected (Benfatto *et al.*, 1997, 2002; Chaboy *et al.*, 2005). The good reproduction of the spectra indicates that, apart from the edge shift, the structural effects are dominant. In other words, the scattering properties of the Mn^{3+} ($LaMnO_3$) and Mn^{4+} ($CaMnO_3$) atoms are very similar and they manifest their presence in the local geometry through the distortion of the MnO_6 octahedra.

The detailed computation performed on both $LaMnO_3$ and $CaMnO_3$ compounds fixes the starting point for evaluating the effect of the chemical substitution through the $La_{1-x}Ca_xMnO_3$ series. With this aim, we have firstly studied the effect of the chemical substitution on the calculation of the Mn *K*-edge XANES spectra in the $La_{1-x}Ca_xMnO_3$ series. Initially, we have considered two situations. In the first model all the La atoms in the $LaMnO_3$ cluster are substituted by Ca ones, but maintaining a fixed crystal structure. In this way we just change the scattering properties of the neighbouring atoms without modifying the MnO_6 arrangement. In the second model we consider a $LaMnO_3$ cluster in which the original distorted Mn—O octahedron (2×1.91, 2×1.97, 2×2.18 Å) around the absorbing atom is substituted by the regular one (4×1.89, 2×1.92 Å) found in $CaMnO_3$. Conversely, similar modifications have been applied to the $CaMnO_3$ cluster: (i) the Ca scatterers have been substituted by La ones, maintaining the crystal structure, and (ii) we have substituted the regular octahedron around the absorbing Mn atom in $CaMnO_3$ by the distorted one of $LaMnO_3$. According to the results summarized in Fig. 2, all the computations have been performed for clusters of 125 atoms, 1% overlapping factor, $l_{max} = 4$ and by using the complex HL exchange and correlation potential (ECP).

The computations, reported in Fig. 3, show two main results regarding the substitution of La by Ca atoms in $LaMnO_3$ and, conversely, of La at the Ca sites in $CaMnO_3$. On the one hand, the intensity of the main absorption peak (or white line) is affected by the substitution. In the case of $LaMnO_3$ it decreases as Ca occupies the La sites. The contrary occurs when La substitutes for Ca in $CaMnO_3$ and then the white line is enhanced. Moreover, the chemical substitution, without changing the MnO_6 octahedra, also affects the shape of the second main resonance as well as its energy position relative to the main absorption line. These results indicate that independently of the local geometry of the first oxygen neighbouring shell the Mn *K*-edge XANES is affected by the type of atoms (La or Ca) located in the second coordination sphere. Consequently, the assumption that the XANES of the intermediate $La_{1-x}Ca_xMnO_3$ compounds could be modelled by simply weighting the spectra of the end-members is not held. Indeed, this simple model would only be valid if the intermediate compounds are a mixture of $LaMnO_3$ and $CaMnO_3$ phases, which is not the case. In a similar way to the above findings, the results reported in Fig. 3 show that for unsubstituted clusters the modification of the MnO_6 geometry also induces significant changes in the intensity, the shape and the relative energy position of the main spectral features. According to these results, the Mn *K*-edge spectra of the partially substituted $La_{1-x}Ca_xMnO_3$ cannot be considered as made by the addition of those of the end-members. The chemical La–Ca substitution implies a modification of the scattering contribution to the XANES spectra. Therefore, the nature of the scatterer (La *versus* Ca), and not only the interatomic distance, plays a non-negligible role.

The next step of our study has been to evaluate the effect of the chemical (La–Ca) substitution on the edge shift. To

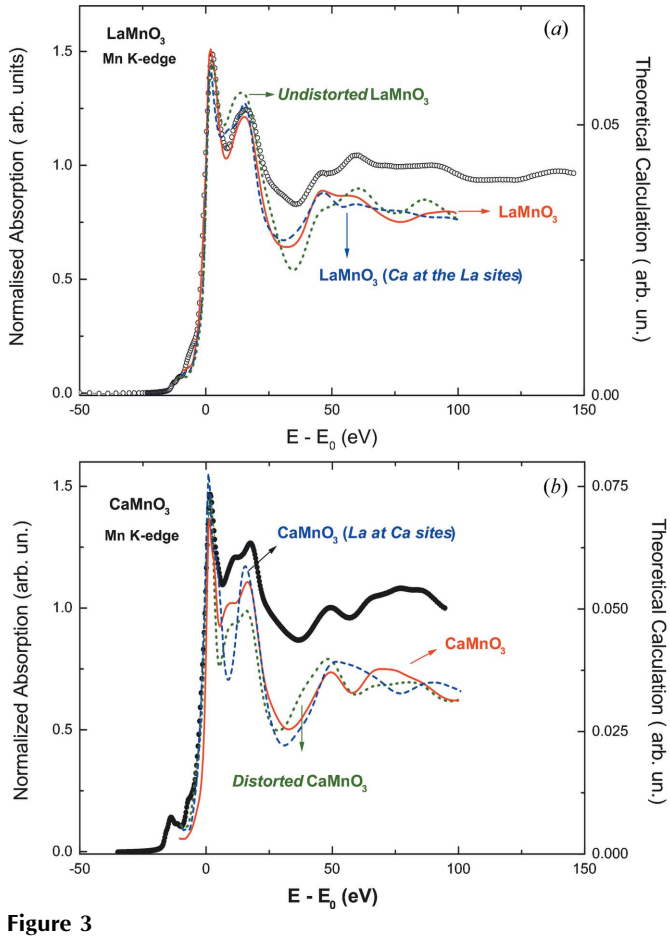

Figure 3
(*a*) Comparison of the experimental XANES spectrum at the Mn *K*-edge (open circles) and the theoretical spectra calculated for a 7 Å cluster of $LaMnO_3$ (red, solid line) and (i) by replacing the La atoms by Ca at the same positions (blue, dashed line) and (ii) by substituting the distorted Mn—O octahedron by the regular one (green, dotted line) as found in $CaMnO_3$ (see text for details). (*b*) Comparison of the experimental XANES spectrum at the Mn *K*-edge (filled circles) and the theoretical spectra calculated for a 7 Å cluster of $CaMnO_3$ (red, solid line) and by substituting the regular Mn—O octahedron by the distorted $LaMnO_3$-like one (blue, dashed line). The computation performed for the same $CaMnO_3$ cluster by replacing the Ca atoms by La at the same positions (green, dotted line) is also shown. This figure is in colour in the electronic version of this paper.

this end, we have computed the Mn *K*-edge XANES spectra for the intermediate $La_{0.67}Ca_{0.33}MnO_3$, $La_{0.5}Ca_{0.5}MnO_3$ and $La_{0.33}Ca_{0.67x}MnO_3$ compounds. It should be noted that the energy scale of each computation is referred to its own muffin-tin potential. Therefore, it is necessary to correct the energy scale of the computed spectra in order to compare the calculations for the different compounds on a unique energy scale prior to account for the edge shift associated with the structural modification.

The experimental Mn *K*-edge spectra of the intermediate $La_{0.67}Ca_{0.33}MnO_3$, $La_{0.5}Ca_{0.5}MnO_3$ and $La_{0.33}Ca_{0.67x}MnO_3$, and those of the end-members (Subías *et al.*, 1997), are shown in Fig. 4. The shift of the threshold between $LaMnO_3$ and $CaMnO_3$ is determined to be $\Delta E = 4.2$ eV by using the first derivative of the spectra. However, this energy difference decreases to 2.7 eV if one looks at the energy position of the

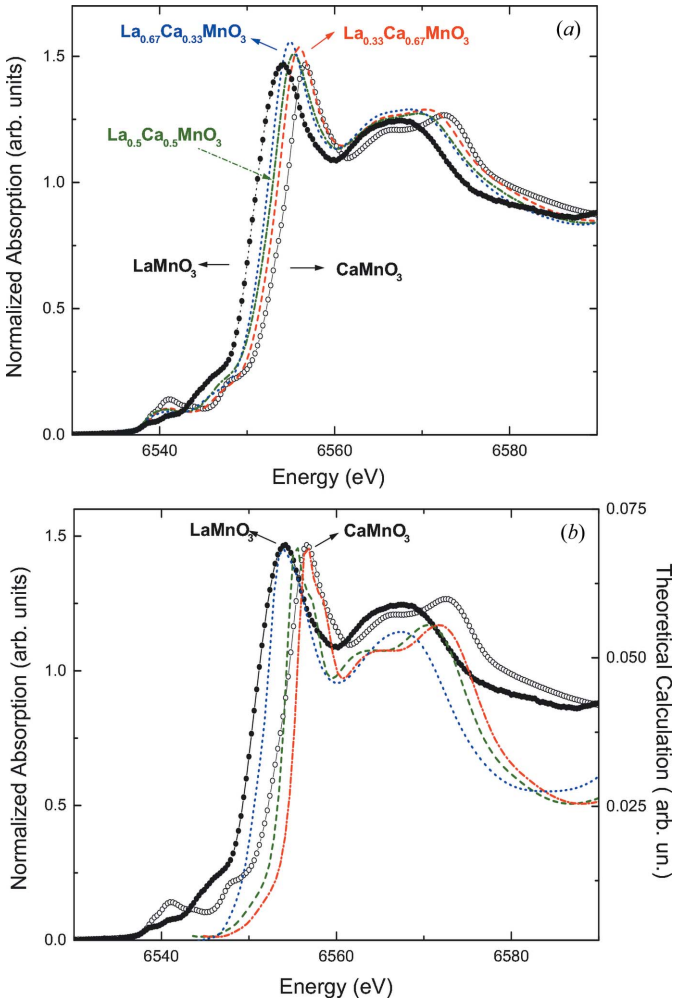

Figure 4
(*a*) Comparison of the experimental XANES spectrum at the Mn *K*-edge through the $La_{1-x}Ca_xMnO_3$ series: $x = 0$ (filled circles), $x = 0.33$ (blue, dotted line), $x = 0.5$ (green, dot-dashed line), $x = 0.67$ (red, dashed line) and $x = 1$ (open circles). (*b*) Comparison of the experimental spectra of $LaMnO_3$ (filled circles) and $CaMnO_3$ (black, open circles) and the result of the computations plotted on a unique absolute energy scale: $LaMnO_3$ (blue, dotted line), $CaMnO_3$ (green, dashed line). The result of shifting by 1 eV the $CaMnO_3$ computation is also shown (red, dot-dashed line). This figure is in colour in the electronic version of this paper.

main absorption peak. The theoretical computations show a similar trend, being $\Delta E = 2.18$ eV and 1.64 eV as determined from the first derivative or the main peak position, respectively. Despite the fact that we are using neutral Mn atoms to perform the calculations, the edge and the energy position of the main absorption line are different for both $LaMnO_3$ and $CaMnO_3$ compounds. This result demonstrates that the different crystal structure contributes to the experimentally observed edge-shift. As discussed above, the experimental energy separation of the main line is 2.7 eV while the neutral-atom computations yield a value of 1.64 eV. By shifting by 1 eV the theoretical spectrum of $CaMnO_3$ with respect to that of $LaMnO_3$, a remarkable agreement with the experimental observations is obtained, as shown in Fig. 4(*b*). These results show that, despite the fact that it is currently assumed that the shift of the absorption edge is associated with a change of the electronic state of Mn, the edge position also depends on the distortion of the MnO_6 octahedron (Benfatto *et al.*, 1999; Qian *et al.*, 2001; Ramos *et al.*, 2007). As recently illustrated by the Mn *K*-edge XANES measurements of $LaMnO_3$ under pressure, the existence of such a distortion does not mean that the electronic state of Mn changes (Ramos *et al.*, 2007). Ramos *et al.* have shown that for pressures above 8 GPa there is a continuous shift of the absorption threshold towards higher energies along with an enhancement of the structures just above the edge (Ramos *et al.*, 2007). Since the manganese formal valence (Mn^{3+}) remains unchanged with pressure, the edge shift (~0.9 eV) and the modification of the main lines in XANES reflect the structural distortion of the MnO_6 octahedra despite the Mn^{3+} state being preserved. These results are in agreement with the work of Benfatto *et al.*, showing that the edge position is mainly determined by the long Mn—O distance (Benfatto *et al.*, 1999), and thus the edge shift is essentially related to the specific reduction in this bond. Moreover, the evolution of the XANES features reflects therefore a continuous reduction of the average JT distortion from 8 GPa up to 15.3 GPa. The evolution of the edge energy as a function of the applied pressure shows that for small shifts the relationship between the reduction of the bond distance and the associated edge shift is almost linear, in agreement with Natoli's rule (Natoli, 1984).

In order to ascertain whether this effect is due to the whole crystal structure, the type of scatterer (La or Ca) or to the distortion of the MnO_6 octahedra, we have compared on the same energy scale the computations reported in Fig. 4 and new calculations performed by considering different Mn—O distortions of the MnO_6 octahedron containing the absorbing Mn atom. In this way we have decreased the distortion of the $LaMnO_3$ octahedron (2×1.93, 2×1.97, 2×2.07 Å), and we have even cancelled this distortion (6×1.97 Å). In both cases the rest of the crystal structure remains unaltered. As shown in Fig. 5, the position of the absorption maximum in $LaMnO_3$ (~10.97 eV) shifts to higher energy (~11.52 eV) as the distortion is reduced and it lies at 11.78 eV in the case of considering the regular MnO_6 octahedron. In addition, if we insert the MnO_6 octahedron of $CaMnO_3$ in the $LaMnO_3$ cluster, the calculation yields a maximum at 13.15 eV, *i.e.* the energy shift is $\Delta E = 2.18$ eV, which coincides with the energy separation of the main peak of the experimental $LaMnO_3$ and $CaMnO_3$ spectra. Finally, we have also investigated the effect of the progressive substitution of La by Ca in the $LaMnO_3$ crystal structure: the MnO_6 octahedra and the interatomic distances remain unchanged and only the number of La–Ca scatterers is modified. As shown in Fig. 6, the edge and both the energy position and the shape of the main spectral features gradually changes as the Ca content increases.

The results of the theoretical calculations reported here demonstrate the existing relationship between the chemical (Ca–La) substitution and both the energy position and the shape of the different spectral features of the Mn *K*-edge XANES spectra in the $La_{1-x}Ca_xMnO_3$ series. Therefore, we have re-examined the model currently used to relate the shift of the absorption edge with the electronic state of the Mn ions

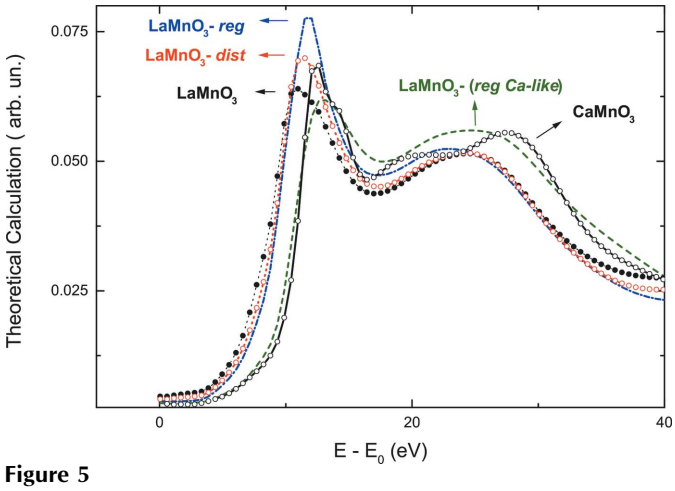

Figure 5
Comparison of the experimental Mn *K*-edge XANES spectrum of $LaMnO_3$ (filled circles) and $CaMnO_3$ (open circles) and the result of the computations, plotted on an absolute energy scale, performed for a 7 Å cluster of $LaMnO_3$ in which the distorted MnO_6 octahedron has been substituted by a regular (red, dotted line) and partly distorted (blue, dot-dashed line) one, and by the same regular one as found in $CaMnO_3$ (green, dashed line) (see text for details). This figure is in colour in the electronic version of this paper.

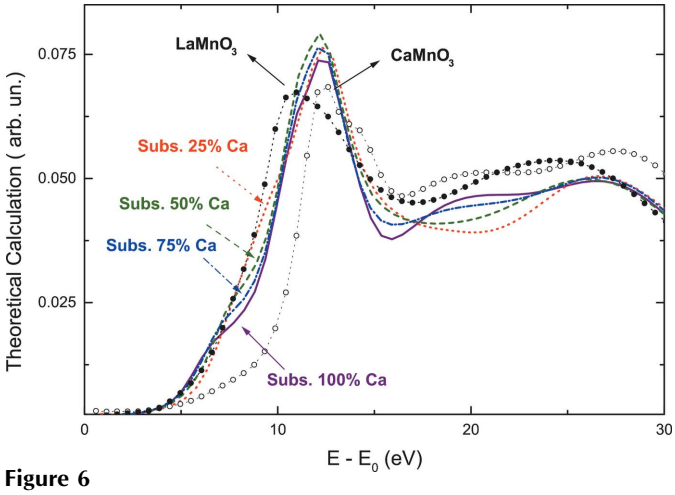

Figure 6
Comparison of the experimental spectra of $LaMnO_3$ (filled circles) and $CaMnO_3$ (black, open circles) and the result of the computations performed for a 7 Å cluster of $LaMnO_3$ in which the La atoms are progressively substituted by Ca: 25% Ca (red, dotted line), 50% (green, dashed line), 75% (blue, dot-dashed line) and 100% (purple, solid line). This figure is in colour in the electronic version of this paper.

through the series. According to this, the XANES spectra of the intermediate-doped compounds was built up by adding, with the appropriate weight, the spectra of $LaMnO_3$ and $CaMnO_3$. The results were not satisfactory and the co-existence of Mn^{3+} and Mn^{4+} ions in the substituted samples was discarded (Booth *et al.*, 1998; Subías *et al.*, 1997; Croft *et al.*, 1997; Bridges *et al.*, 2001). However, the results of our calculations indicate that the distortion of the MnO_6 octahedra affects both the edge position and the spectral shape. Consequently, the Mn *K*-edge absorption shifts in energy as a function of the La–Ca substitution through the series. Starting from the $LaMnO_3$ limit, the distortion of the MnO_6 octahedra decreases as the Ca content increases, shifting the edge towards higher energies. The contrary occurs when $CaMnO_3$ is considered: as La substitutes for Ca the original regular octahedra become distorted, shifting the edge towards lower energies. Then, we have corrected the naive model by incorporating these energy shifts. In this way, the XANES spectra of the intermediate compounds are calculated as the weighted sum of those of $LaMnO_3$ and $CaMnO_3$, in its adequate proportion, but after applying the appropriate energy-shift corresponding to the distortion. This is illustrated in Figs. 7 and 8 in the case of $La_{0.5}Ca_{0.5}MnO_3$ and $La_{0.33}Ca_{0.67x}MnO_3$, respectively. According to our computations, the energy shift between the spectra of $LaMnO_3$ and $CaMnO_3$ is 2 eV. Then, in

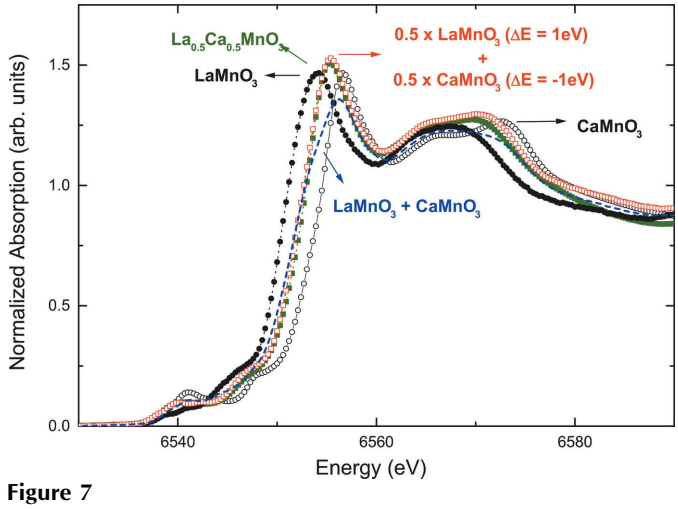

Figure 7
Comparison of the experimental XANES spectrum at the Mn *K*-edge of $LaMnO_3$ (black, filled circles), $La_{0.5}Ca_{0.5}MnO_3$ (green, filled squares) and $CaMnO_3$ (black, open circles), with the averaged sum (50:50) of the end-members spectra (blue, dashed line). In addition, the result of adding the spectra of both $LaMnO_3$ and $CaMnO_3$ after applying a shift of 1 eV and −1 eV, respectively, is also shown (red, open squares). This figure is in colour in the electronic version of this paper.

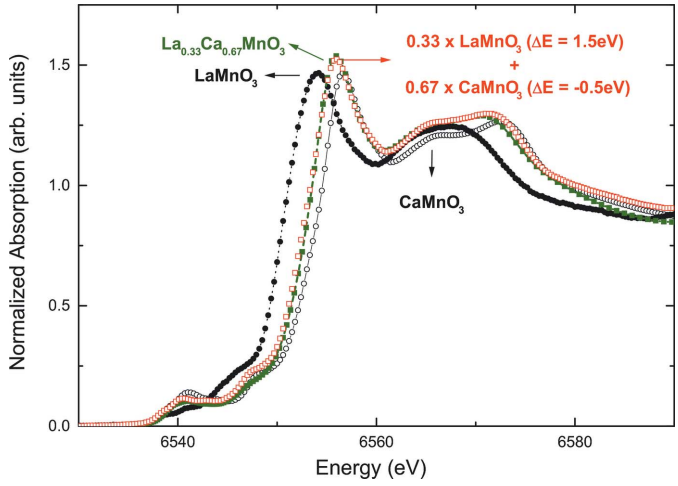

Figure 8
Comparison of the experimental XANES spectrum at the Mn *K*-edge of $LaMnO_3$ (black, filled circles), $La_{0.33}Ca_{0.67}MnO_3$ (green, filled squares) and $CaMnO_3$ (black, open circles), with the weighted sum (0.33:0.67) of the $LaMnO_3$ and $CaMnO_3$ after applying a shift of 1.5 eV and −0.5 eV, respectively (red, open squares). This figure is in colour in the electronic version of this paper.

the case of $La_{0.5}Ca_{0.5}MnO_3$ we have shifted the spectrum of $LaMnO_3$ by 1 eV and that of the $CaMnO_3$ by −1 eV. The result of this procedure is shown in Fig. 7, where the weighted signal has been multiplied by 1.04 to match the intensity of the main peak. The agreement between the experimental spectrum and the signal constructed starting from the end-members is remarkable. Finally, we have applied an identical procedure to the $La_{0.33}Ca_{0.67}MnO_3$ compound for which charge ordering has been claimed. In this case, the spectrum of $LaMnO_3$ has been shifted by 1.5 eV and that of $CaMnO_3$ by −0.5 eV. After applying the appropriate weighting, the obtained signal matches the experimental spectrum as shown in Fig. 8. Therefore, contrary to previous assignments, the experimental Mn *K*-edge XANES spectra of the $La_{1-x}Ca_xMnO_3$ compounds support the existence of well defined Mn^{3+} and Mn^{4+} ions, *i.e.* distorted and undistorted octahedra. These results are in agreement with the analysis of Booth *et al.*, showing that, as the calcium concentration increases, the oxygen environment around the manganese becomes less distorted, these Mn—O distortions being consistent with a model which includes a JT distortion in proportion to the Ca concentration (Booth *et al.*, 1998).

4. Summary and conclusions

We have reported an extensive and systematic *ab initio* computation of the Mn *K*-edge in $LaMnO_3$, $CaMnO_3$ and the intermediate $La_{1-x}Ca_xMnO_3$ compounds performed within the multiple-scattering framework.

We have shown the need to use big clusters in order to reproduce all the spectral features, as well as the correct energy position and intensity ratio. In particular, the comparison between the experimental data and the theoretical calculations has demonstrated the need to use large clusters, ∼7 Å around the central photoabsorbing atom, to reproduce the experimental spectra alloys. These needs are independent of the electronic state of the Mn atoms and of the occurrence of distorted or undistorted MnO_6 octahedra through the series.

By fixing the same computational parameters we have studied the relationship between the edge shift, the Ca–La substitution and the distortion of the MnO_6 octahedra. It is shown that by correctly considering these effects simultaneously the experimental XANES data are consistent with the presence of two different Mn local environments through the $La_{1-x}Ca_xMnO_3$ series. In addition, by taking into account the energy shift associated with the modification of the MnO_6 distortion as Ca substitutes for La, it is shown that it is possible to reproduce the XANES spectra of the intermediate-doped compounds starting from the experimental spectra of the end-member $LaMnO_3$ and $CaMnO_3$ compounds. These results point out the need to re-examine the conclusions derived in the past from simple analysis of the Mn *K*-edge XANES shift in these materials. In particular, we show that the modification of the Mn *K*-edge absorption through the $La_{1-x}Ca_xMnO_3$ series is well accounted for by considering the simultaneous presence of both distorted and undistorted octahedra and, consequently, the existence of charge ordering phenomena cannot be ruled out based on the XANES data. The results reported here solve the perennial issue of similar XAS experimental results leading to opposite conclusions.

APPENDIX *A*
Computation of the Mn *K*-edge XANES

Here we present the details of the *ab initio* Mn *K*-edge XANES calculations performed in the case of both $LaMnO_3$ and $CaMnO_3$, *i.e.* the end-members of the $La_{1-x}Ca_xMnO_3$ series. For the computations we have used the crystallographic data of $LaMnO_3$ and $CaMnO_3$ reported by Iliev *et al.* (1998) and Fawcett *et al.* (1998), respectively.

Initially, we have built up a $LaMnO_3$ cluster containing 69 atoms, *i.e.* including contributions from atoms located within the first ∼5.5 Å around Mn. We have tested for this fixed-size cluster the effect of modifying the value of the maximum angular momentum quantum number, l_{max}, needed to account for the experimental absorption spectrum in the first 60 eV. As shown in Fig. 9, computations performed by using low l_{max} values fail to reproduce the experimental spectral shape. While the experimental spectrum shows a well defined energy separation between the main absorption peak (A) and the first broad resonance centred at ∼16 eV (B), the l_{max} = 3 computation exhibits an asymmetric profile in which the broad resonance is attached to the main peak. Moreover, feature C is not reproduced at all and the calculated absorption minima and maxima fall short of the observed ones, which is evident in the case of the absorption minimum between features C and D. In this respect, it should be noted that the comparison of the computed spectrum and the experimental one is limited by the angular momentum expansion of the global scattering function ($l_{max} \simeq kR$, where R is the smallest atomic sphere radii and l_{max} is the maximal momentum for partial waves used inside atomic spheres). Then, we have increased l_{max} to 4. In this way a better expansion of the angular momentum within

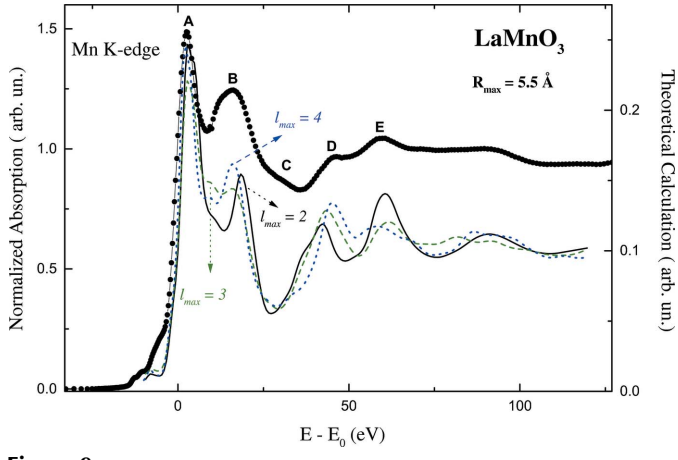

Figure 9
Comparison of the experimental XANES spectrum at the Mn *K*-edge in $LaMnO_3$ (filled circles) and the theoretical spectra calculated on a 5.5 Å cluster by using real HL ECP potential and different l_{max} values: l_{max} = 2 (black, solid line), l_{max} = 3 (green, dashed line) and l_{max} = 4 (blue, dotted line). This figure is in colour in the electronic version of this paper.

the La spheres is obtained and, moreover, the energy range in which the computation can be compared with the experimental spectrum is increased. Fig. 9 shows the improvement of this computation: the main spectral features, A and B, are now well energy-resolved and, in addition, a better energy position of the high-energy feature D (∼45 eV) is obtained.

However, despite the above progress, both the shape and the width of the second resonance (B) are still poorly accounted for by the computation that, in addition, yields the absorption minimum ∼8 eV below the experimental (∼36 eV) value. Therefore, we have increased the cluster size in order to obtain a better reproduction of the experimental spectrum. Previous works have reported computations performed on a cluster of 87 atoms (Ignatov *et al.*, 2001; Qian *et al.*, 2001; Monesi *et al.*, 2005). Such a cluster covers contributions of atoms within the first 6.125 Å around the absorbing atom. The added coordination shells only include O atoms so that no large differences are expected with respect to the computation for the 5.8 Å cluster reported in Fig. 9. The next neighbouring shells, not included in the 87 atoms cluster, correspond to 24 La (∼6.4 Å) and 8 Mn (∼6.7 Å) atoms. For these shells a greater contribution to the scattering processes compared with that of the O atoms is expected. Therefore, we have performed the computations for clusters including these contributions (119 atoms) and for a bigger one containing 295 atoms. In the last case, all the contributions within the first 9.5 Å around the central Mn are included. For these computations we have used only the real part of the Hedin–Lundqvist complex potential (hereafter, real HL). The reason for this is to avoid the possibility of introducing an excessive damping of the excited photoelectron that can smear the appearance of new contributions to the XANES spectrum coming from the addition of further coordination shells.

As shown in Fig. 10, increasing the cluster size from 87 to 119 atoms slightly improves the computations. By contrast, the use of the biggest cluster (295 atoms) significantly improves the results: (i) the intensity ratio between the A and B features, ∼1.15, approaches the experimental one (∼1.2) whereas it is ∼1.84 for the smaller clusters; (ii) the width and the asymmetric shape of feature B are well reproduced; (iii) the energy position of features E and D matches those observed experimentally; (iv) the computation accounts for the feature C located at the high energy part of the broad B peak, that was missed in the former calculations. Finally, we have also checked the importance of the choice of the overlapping factor among the muffin-tin spheres in the correct reproduction of the absorption spectrum. Our results show that it influences both the intensity and the spectral shape in the first 40 eV of the computed spectra, which results crucially in correctly reproducing the broad resonance B of the $LaMnO_3$ spectrum. In this respect, computations performed by using a 1% factor show a better agreement with the experimental spectrum than those corresponding to a 10% overlapping factor (see inset of Fig. 10).

The results of the calculations performed by using only the real part of the HL ECP point out the need to use quite big clusters in order to reproduce the experimental spectrum of

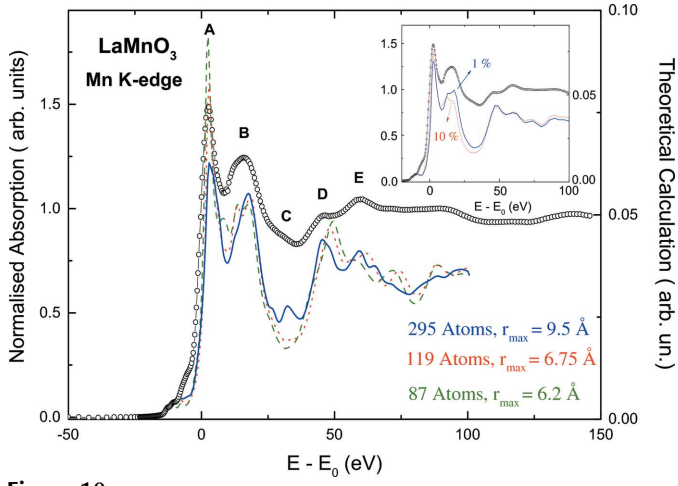

Figure 10
Comparison of the experimental XANES spectrum at the Mn *K*-edge in $LaMnO_3$ (open circles) and the theoretical spectra calculated cluster by imposing an overlapping factor of 1%, $l_{max} = 4$ and the real part of the HL potential on clusters of increasing size (87, 119 and 295 atoms) covering up to 6 Å (green, dashed line), 6.75 (red, dotted line) and 9.5 Å (blue, solid line) around the absorbing Mn atom. In the inset, a comparison of the computation performed on the 119 atoms cluster by imposing an overlapping factor of 1% (blue, solid line) and 10% (red, dotted line) is shown. This figure is in colour in the electronic version of this paper.

$LaMnO_3$. However, the relative intensity of the spectral features is not in agreement with those observed experimentally, as expected, because the photoelectron damping was not taken into account in the real HL calculations. Consequently, we have conducted a similar computational procedure as above but using the complex HL ECP potential. As in the case of using the real HL, the importance of the scattering processes involving atoms located beyond the first 6 Å around the absorbing Mn is fundamental in order to reproduce the shape and the intensity of the experimental spectrum. As shown in Fig. 11(*a*), the agreement between the experimental and theoretical spectrum is not satisfactory when the computations are performed for medium-size, $r_{max} \leq 6$ Å, clusters. The best reproduction of the experimental spectrum is obtained for a cluster made of 295 atoms. The computation made by using this cluster and $l_{max} = 4$ yields an accurate reproduction of the high-energy spectral features in the first 50 eV above the edge. Based on these results and in order to reduce the computational time, we have studied the minimum cluster size needed to account for the experimental spectrum. As shown in Fig. 11(*b*), no significant differences are found among the computations performed on clusters including the coordination spheres within the first 7 Å (125 atoms), 8 Å (167) and 9.5 Å (295) around the absorbing Mn. Therefore, we conclude that the minimum size of the cluster needed to account for the Mn *K*-edge XANES of $LaMnO_3$ has to include all the neighbours within the first 7 Å around the absorbing Mn atom.

Despite the fact that the agreement between the experimental and the theoretical spectra is remarkable, several problems remain in the high-energy region. Indeed, the computed energy position and the relative intensity of the high-energy features D and E do not match those observed

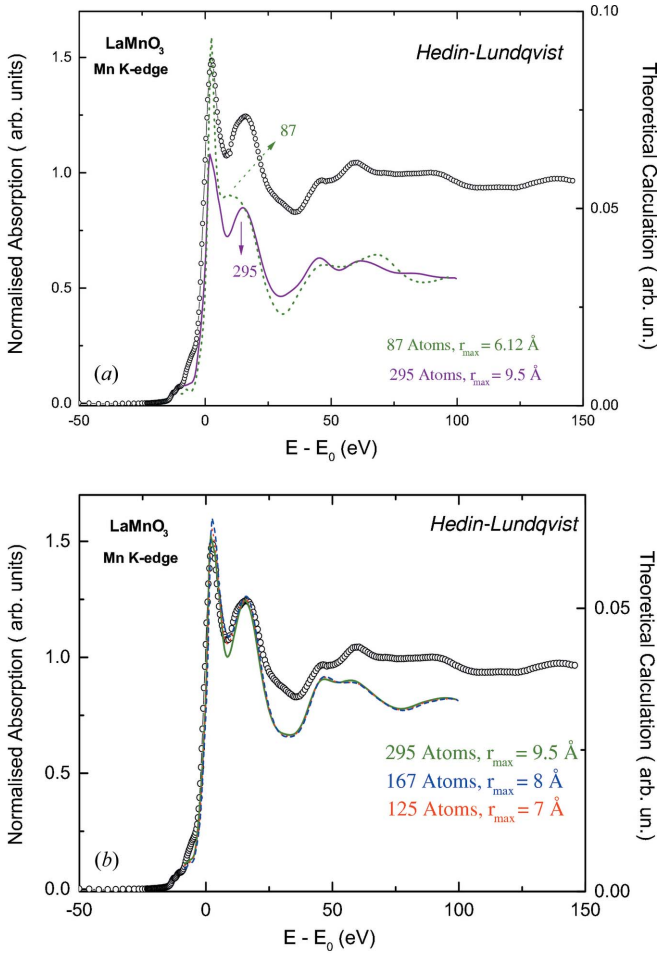

Figure 11
(*a*) Comparison of the experimental XANES spectrum at the Mn *K*-edge in $LaMnO_3$ (open circles) and the theoretical spectra calculated by imposing an overlapping factor of 1%, $l_{max} = 3$, and by using the complex HL potential in clusters of 87 atoms (green, dotted line) and 295 atoms (purple, solid line). (*b*) Comparison of the computations performed by using $l_{max} = 4$ on clusters containing 125 atoms ($r_{max} = 7$ Å) (red, dotted line), 167 atoms ($r_{max} = 8$ Å) (blue, dashed line) and 295 atoms ($r_{max} = 9.5$ Å) (green, solid line). This figure is in colour in the electronic version of this paper.

experimentally. We have attempted to improve this result by modifying the exchange and correlation potential used in the computations. In this way we have verified that the energy-dependent DH exchange potential (Natoli *et al.*, 2003) improves the computations in such a way that the energy position of the energy minimum (~36 eV above the edge) and of both peaks E (~45 eV) and D (~60 eV) is now properly accounted for. However, with the DH being a real potential, the intensity of the computed spectral features is too high, as previously obtained for the real HL case. We have added to the DH ECP the imaginary part of the HL one (hereafter, complex DH) in order to account for the photoelectron damping. As shown in Fig. 12, the agreement between the theoretical calculation and the experimental spectrum is excellent in the first 65 eV above the edge, especially regarding the high-energy spectral features.

The results reported in the previous section show the necessary conditions for obtaining an accurate reproduction of

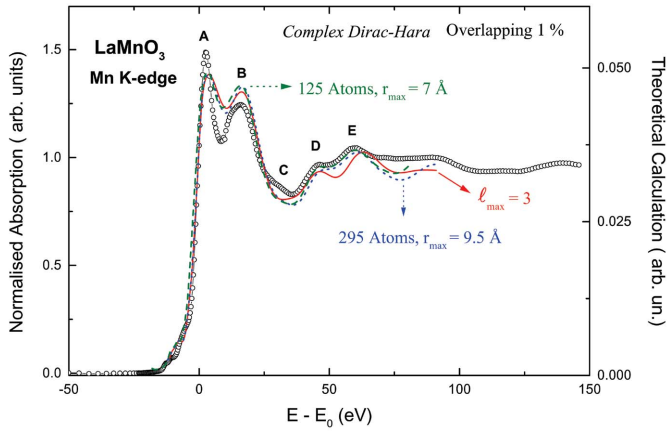

Figure 12
Comparison of the experimental XANES spectrum at the Mn *K*-edge in $LaMnO_3$ (open circles) and the theoretical spectra calculated cluster by using the complex DH potential on two clusters containing 125 atoms, $r_{max} = 7$ Å (green, dashed line) and 295 atoms, $r_{max} = 9.5$ Å, (blue, dotted line). The computations were made by imposing an overlapping factor of 1% and $l_{max} = 4$. For the sake of completion the calculation performed on the biggest cluster by using $l_{max} = 3$ (red, solid line) is also shown. This figure is in colour in the electronic version of this paper.

the experimental Mn *K*-edge XANES spectra in the $La_{1-x}Ca_xMnO_3$ systems. The conducted methodology pays special attention to several computational aspects that are sometimes overlooked leading to incorrect conclusions because of the inappropriate use of the computer tools. It should be stressed that no fitting parameter has been used during the calculations. The theoretically calculated spectra have been directly compared with the experimental XANES spectrum, *i.e.* no fitting procedure has been used. Recently, a good agreement between the experimental and computed data has been reported for $LaMnO_3$ and $CaMnO_3$ (Monesi *et al.*, 2005; Monesi, 2006) by using a fitting procedure of the parameters which describes both the potential and the structure, and by including an *ad hoc* energy-dependent broadening. Moreover, a double excitation feature was included during the fitting at 69.4 eV and 75.4 eV for La and Ca compounds, respectively. However, XAS and X-ray magnetic circular dichroism measurements determine that the onset of this secondary channel lies at ~45 eV above the edge (Subías *et al.*, 2005, 2007). As a result, the parameters used for the computation of both $LaMnO_3$ and $CaMnO_3$ significantly differ (Monesi, 2006) and prevent studying of the relationship between the structural distortion and the Mn valence under this fitting approach.

Consequently, we adopt the same prescriptions to compute the Mn *K*-edge of $CaMnO_3$. The results, reported in Fig. 13, show that the effect of the cluster size on the calculations is the same as in the case of $LaMnO_3$. By using the standard 87 atoms cluster, the experimental intensity ratio of the two peaks B_1 and B_2 is not accounted for by the calculation. On the contrary, the computation yields both the correct shape and intensity ratio when a cluster containing 125 atoms is used. While in the case of $LaMnO_3$ such a cluster includes contributions from neighbouring atoms located within the first 7 Å around the absorbing Mn atom, it ranges only by ~6.6 Å

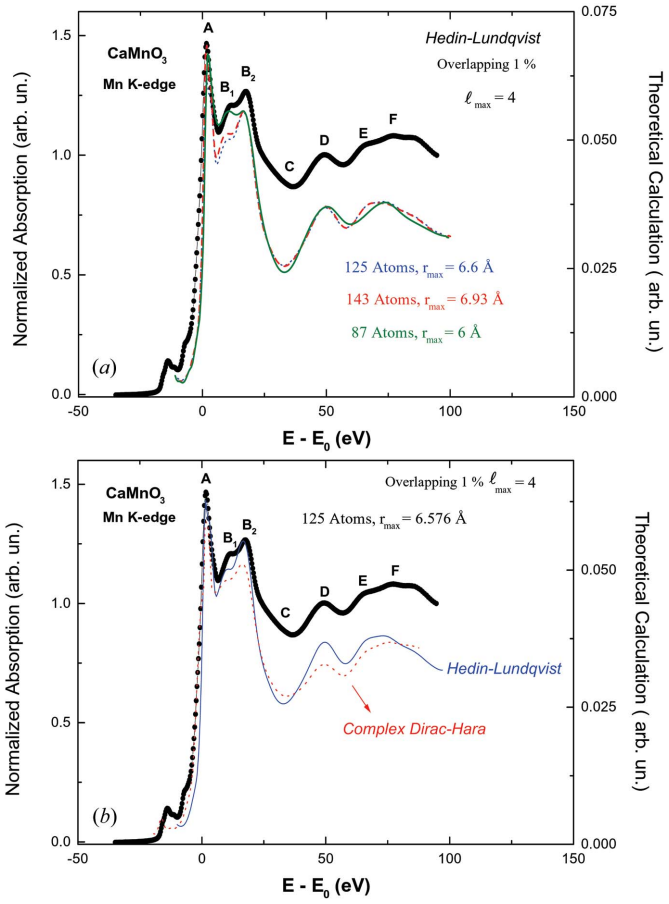

Figure 13
(*a*) Comparison of the experimental XANES spectrum at the Mn *K*-edge in $CaMnO_3$ (filled circles) and the theoretical spectra calculated for different cluster sizes: (green, solid line) 87 atoms (r_{max} = 6 Å); (blue, dotted line) 125 atoms (r_{max} = 6.6 Å); (red, dashed line) 143 atoms (r_{max} = 7 Å). (*b*) Comparison of the computations performed on the 125 atoms cluster by using both complex HL (blue, solid line) and DH (red, dotted line) potentials. This figure is in colour in the electronic version of this paper.

in the case of $CaMnO_3$. Therefore, we have extended the computation to a $CaMnO_3$ cluster including these contributions, *i.e.* r_{max} = 7 Å. However, as shown in Fig. 13(*a*), no significant difference is found between the computations performed on both 125 and 143 atom clusters. As in the case of $LaMnO_3$, the use of complex potentials leads to the best reproduction of the experimental spectrum, regarding both the energy position and the intensity of the experimentally observed spectral features in the first 70 eV above the absorption edge (Fig. 13*b*).

This work was partially supported by the Spanish CICYT MAT2005-06806-C04-04 and MAT2008-06542-C04-01 grants. G. Subías is acknowledged for providing the original experimental spectra reported (Subías *et al.*, 1997).

References

Anderson, P. & Hasegawa, H. (1955). *Phys. Rev.* **100**, 675–681.
Ankudinov, A., Ravel, B., Rehr, J. J. & Conradson, S. D. (1998). *Phys. Rev. B*, **58**, 7565–7566.
Benfatto, M., Joly, Y. & Natoli, C. R. (1999). *Phys. Rev. Lett.* **83**, 636–639.
Benfatto, M., Natoli, C. R., Bianconi, A., García, J., Marcelli, A., Fanfoni, M. & Davoli, I. (1986). *Phys. Rev. B*, **34**, 5774–5778.
Benfatto, M., Solera, J. A., Chaboy, J., Proietti, M. G. & García, J. (1997). *Phys. Rev. B*, **56**, 2447–2452.
Benfatto, M., Solera, J. A., García, J. & Chaboy, J. (2002). *Chem. Phys.* **282**, 441–450.
Booth, C. H., Bridges, F., Kwei, G. H., Lawrence, J. M., Cornelius, A. L. & Neumeier, J. J. (1998). *Phys. Rev. B*, **57**, 10440–10454.
Booth, C. H., Bridges, F., Snyder, G. J. & Geballe, T. H. (1996). *Phys. Rev. B*, **54**, R15606–R15609.
Bridges, F., Booth, C. H., Anderson, M., Kwei, G. H., Neumeier, J. J., Snyder, J., Mitchell, J., Gardner, J. S. & Brosha, E. (2001). *Phys. Rev. B*, **63**, 214405.
Chaboy, J., Muñoz-Páez, A., Carrera, F., Merkling, P. & Sánchez Marcos, E. (2005). *Phys. Rev. B*, **71**, 134208.
Chaboy, J. & Quarteri, S. (1995). *Phys. Rev. B*, **52**, 6349–6357.
Chen, C. H., Cheong, S. W. & Hwang, H. Y. (1997). *J. Appl. Phys.* **81**, 4326.
Clementi, E. & Roetti, C. (1974). *Atom. Data Nucl. Data Tables*, **14**, 177–478.
Croft, M., Sills, D., Greenblatt, M., Lee, C., Cheong, S. W., Ramanujachary, K. V. & Tran, D. (1997). *Phys. Rev. B*, **55**, 8726–8732.
Dagotto, E., Hottta, T. & Moreo, A. (2001). *Phys. Rep.* **344**, 1–153.
Desclaux, J. P. (1975). *Comput. Phys. Commun.* **9**, 31–45.
Edwards, D. M. (2002). *Adv. Phys.* **51**, 1259–1318.
Elfimov, I. S., Anisimov, V. I. & Sawatzky, G. A. (1999). *Phys. Rev. Lett.* **82**, 4264–4267.
Fawcett, I., Sunstrom, J. E. I., Greenblatt, M., Croft, M. & Ramanujachary, K. V. (1998). *Chem. Mater.* **10**, 3643–3651.
García, J., Sánchez, M. C., Blasco, J., Subías, G. & Proietti, M. G. (2001*a*). *J. Phys. Condens. Matter*, **13**, 3243–3256.
García, J., Sánchez, M. C., Subías, G. & Blasco, J. (2001*b*). *J. Phys. Condens. Matter*, **13**, 3229–3241.
Gennes, P. de (1960). *Phys. Rev.* **118**, 141–154.
Ignatov, A. Y., Ali, N. & Khalid, S. (2001). *Phys. Rev. B*, **64**, 014413.
Iliev, M. N., Abrashev, M. V., Lee, H. G., Popov, V. N., Sun, Y. Y., Thomsen, C., Meng, R. L. & Chu, C. W. (1998). *Phys. Rev. B*, **57**, 2872–2877.
Jiang, Y., Bridges, F., Downward, L. & Neumeier, J. J. (2007). *Phys. Rev. B*, **76**, 224428.
Krause, M. O. & Oliver, J. H. (1979). *J. Phys. Chem. Ref. Data*, **8**, 329–338.
Lanzara, A., Saini, N. L., Brunelli, M., Natali, F., Bianconi, A., Radaelli, P. G. & Cheong, S. W. (1998). *Phys. Rev. Lett.* **81**, 878–881.
Lee, P. A. & Beni, G. (1977). *Phys. Rev. B*, **15**, 2862–2883.
Lee, P. A. & Pendry, J. B. (1975). *Phys. Rev. B*, **11**, 2795–2811.
Louca, D. & Egami, T. (1999). *Phys. Rev. B*, **59**, 6193–6204.
Mattheis, L. F. (1964). *Phys. Rev.* **133**, A1399–A1403.
Meneghini, C., Castellano, C., Mobilio, S., Kumar, A., Ray, S. & Sarma, D. D. (2002). *J. Phys. Condens. Matter*, **14**, 1967–1974.
Meneghini, C., Cimino, R., Pascarelli, S., Mobilio, S., Raghu, C. & Sarma, D. D. (1997). *Phys. Rev. B*, **56**, 3520–3523.
Millis, A. J., Littlewood, P. B. & Shraiman, B. I. (1995). *Phys. Rev. Lett.* **74**, 5144–5147.
Millis, A. J., Shraiman, B. I. & Mueller, R. (1996). *Phys. Rev. Lett.* **77**, 175–178.
Monesi, C. (2006). PhD Thesis. Università degli Studi Roma Tre, Italy.
Monesi, C., Meneghini, C., Bardelli, F., Benfatto, M., Mobilio, S., Manju, U. & Sarma, D. D. (2005). *Phys. Rev.* **72**, 174104.
Murakami, Y., Kawada, H., Kawata, H., Tanaka, M., Arima, T., Moritomo, Y. & Tokura, Y. (1998). *Phys. Rev. Lett.* **80**, 1932–1935.
Nakamura, K., Arima, T., Nakazawa, A., Wakabayashi, Y. & Murakami, Y. (1999). *Phys. Rev. B*, **60**, 2425–2428.
Natoli, C. R. (1984). *EXAFS and Near Edge Structure III, Springer Proceedings in Physics*, Vol. 2, p. 38. Berlin: Springer-Verlag.

Natoli, C. R. & Benfatto, M. (1986). *J. Phys. Paris Colloq.* **47**, C8–11.
Natoli, C. R., Benfatto, M., Della Longa, S. & Hatada, K. (2003). *J. Synchrotron Rad.* **10**, 26–42.
Norman, J. G. (1974). *Mol. Phys.* **81**, 1191–1198.
Qian, Q., Tyson, T. A., Kao, C. C., Croft, M., Cheong, S. W., Popov, G. & Greenblatt, M. (2001). *Phys. Rev. B*, **64**, 024430.
Radaelli, P. G., Iannone, G., Marezio, M., Hwang, H. Y., Cheong, S. W., Jorgensen, J. D. & Argyriou, D. N. (1997). *Phys. Rev. B*, **56**, 8265–8276.
Ramirez, A. P., Schiffer, P., Cheong, S. W., Chen, C. H., Bao, W., Palstra, T. M., Gammel, P. L., Bishop, D. J. & Zegarski, B. (1996). *Phys. Rev. Lett.* **76**, 3188–3191.
Ramos, A. Y., Tolentino, H. C. N., Souza-Neto, N. M., Itié, J. P., Morales, L. & Caneiro, A. (2007). *Phys. Rev. B*, **75**, 052103.
Renner, C., Kim, B. G. & Cheng, S. W. (2002). *Nature (London)*, **416**, 518–521.
Salamon, B. & Jaime, M. (2001). *Rev. Mod. Phys.* **73**, 583–628.
Schiffer, P., Ramirez, A. P., Bao, W. & Cheong, S. W. (1995). *Phys. Rev. Lett.* **75**, 3336–3339.
Subías, G., Chaboy, J., Laguna-Marco, M. A., García, J., Luis, F., Maruyama, H. & Kawamura, N. (2005). *SPring8 User Exp. Rep.* **15**, 183.
Subías, G., García, J., Blasco, J. & Proietti, M. G. (1998). *Phys. Rev. B*, **58**, 9287–9293.
Subías, G., García, J., Blasco, J., Sánchez, M. C. & Proietti, M. G. (2002). *J. Phys. Condens. Matter*, **14**, 5017–5033.
Subías, G., García, J., Proietti, M. G. & Blasco, J. (1997). *Phys. Rev. B*, **56**, 8183.
Subías, G., García, J. & Sánchez, M. C. (2007). *AIP. Conf. Proc.* **882**, 783–785.
Zener, C. (1951). *Phys. Rev.* **82**, 403–405.
Zimmermann, M. v., Hill, J. P., Gibbs, D., Blume, M., Casa, D., Keimer, B., Murakami, Y., Tomioka, Y. & Tokura, Y. (1999). *Phys. Rev. Lett.* **83**, 4872–4875.